A Study of the CTHA Based on Analytical Models

Douglas B. Miron, *Senior Member, IEEE*

Abstract—The first electromagnetic analysis of the contra-wound toroidal helix antenna (CTHA) is presented. This very-low-profile antenna is seen to have characteristics derivable from a transmission line with a standing current wave and an array of small loops. Formulas for the far-field radiation and efficiency are given. These are used, in conjunction with a numerical model, to develop some trends relating performance and design parameters.

Index Terms—Helical antennas.

I. INTRODUCTION

A. Background and Motivation

THE contra-wound toroidal helix antenna (CTHA) is formed by placing two spiral windings on a toroid core, as shown in Fig. 1. It is generally built as an electrically-small, very-low-profile antenna. It has the interesting property that it can be designed to have nearly isotropic radiated power density. It was invented at West Virginia University [1], [2] but has not received a fundamental treatment through electromagnetic theory before now. The analysis reported in this paper was done in 1996 [3] and deals only with the case of an air core. The purpose of this work is to provide as much insight as possible from an analytic point of view, both for its own sake and to serve as a reference for comparison with numerical and experimental studies. The most desirable situation is to have results that agree from analysis, simulation, and physical experiment, but each area has its limitations and hazards so that comparisons should be made and work revisited in each approach until the differences are either reconciled or at least understood.

B. Basic Geometry and Character

It is helpful to think of the windings in several ways. The first way begins with the upper source terminal in Fig. 1. Start with the wire going up and to the right, follow it around, and see that it comes back to the source from the lower left. Likewise, again starting from the upper source terminal, follow the wire that goes up and to the left, and see that it comes back to the source from the lower right. The wires are insulated, so that their only conductive connections are at the source terminals. Then each winding looks like a conventional helix whose axis has been bent into a loop, and the winding terminates electrically at the source instead of in an open circuit as in the case of a conventional helix. A straight-axis electrically-small helix is usually viewed as radiating as if it were made up of a sequence of alternating small loops and small linear current elements (dipoles)
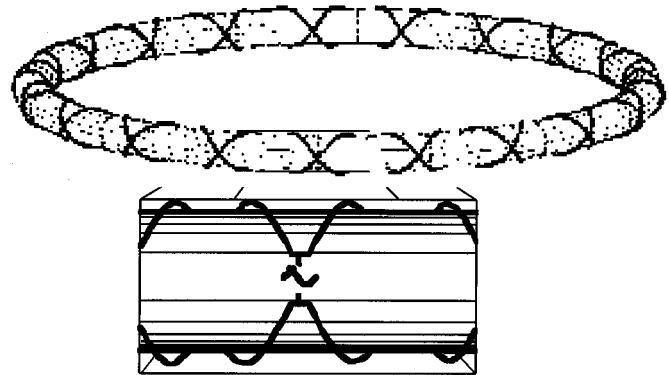
Fig. 1. Perspective view of a CTHA, with an exploded view of a feedpoint.

[4, p. 334ff]. The linear current elements radiate waves whose electric vector is parallel to the helix axis, while the loops radiate waves whose electric vector is parallel to the plane of the loop, perpendicular to the helix axis. Wrapping a helix on a toroid instead of a cylinder means that the linear current elements will be formed in a single larger loop and this loop will radiate a wave with its electric vector parallel to the plane of the toroid (horizontal for this discussion). The effect of the second winding on the CTHA is to produce a second wave, from the axial components of current, whose horizontal electric field is opposite to that of the first winding, producing no net horizontal electric field. This effect can be seen in Fig. 2, which shows the reference directions for currents in the two windings. Looking at any two adjacent wires on the top, one can see that their resultant is a current that passes straight across the top, and likewise, the currents passing underneath have a resultant lying on a radius line of the torus. Except for distortions of the winding, there would be no equivalent current parallel to the toroid centerline (the bent helix winding axis), and therefore no E vector in the plane of the toroid. One can also see that under each half-turn of one winding, there is a half-turn of the other winding. These two half-turns have the same current in opposite directions so that they are equivalent to a single complete vertical loop with an approximately elliptic shape. From this, we conclude that an adequate way of treating the CTHA for finding its radiation field is to treat each pair of half-turns as a single-turn vertical loop of elliptical shape with a space orientation determined by its position on the toroid.

A second way of viewing the windings is to see that both of the wires leaving the source to the right form a transmission line, something like a twisted-pair phone line. This line goes around and connects, in a cross-tied manner, to itself, so that the source both drives and terminates the line. However, from the previous figures, it is clear that the current distribution has symmetry about the source, and in fact about a diameter line
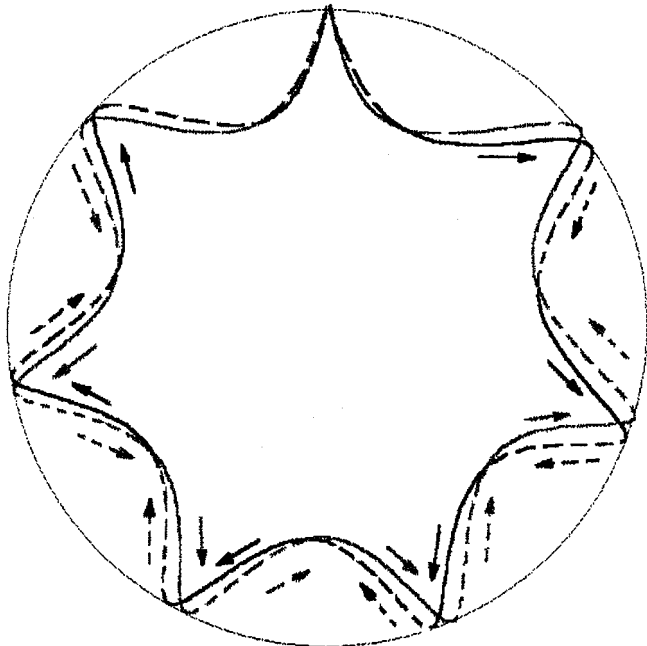
Fig. 2. Top view of a CTHA winding. The arrows show reference current directions. Solid arrows and lines are on the top half, broken arrows and lines are on the bottom half. Observe that each top half-turn of one winding lies over a bottom half-turn of the other winding, and the currents in each such pair are equal and opposite. This makes each such pair an equivalent loop with current circulating around the core.

of the antenna passing through the source to the opposite point on the line, halfway around the winding. Therefore, it is more useful to think of the windings as two transmission lines driven in parallel at the source, going left and right around the toroid, and terminating at a cross-tie on the far side. Because of the cross-tie, the lines short each other. A transmission line with a short circuit termination has a standing-wave current distribution on it. If it weren't for losses, the total current would be a sine function of position on the line. Also, such a structure has resonances. The input impedance must be inductive at frequencies below the first resonance, just as in a conventional shorted line. The first resonance will be a high-impedance transition between inductive and capacitive reactance, the second resonance will be a low-impedance transition from capacitive back to inductive reactance, and so on.

It is not possible to obtain analytical relations between the CTHA geometry and the transmission-line parameters. An approach that allows a qualitative understanding of the impedance behavior is to view the windings as a periodic structure, with each loop having some inductance, wire resistance, shunt capacitance (mostly from the wire crossings), and mutual inductance with the loops on either side. A circuit analysis based on these ideas is given in [3] but is omitted in this paper since it has no bearing on the antenna performance treatment.

C. Analysis Assumptions and Approaches

The ideas in the preceding paragraphs are the basis for the analysis given in the following sections. Each radiating loop is assumed to have a constant current whose value is a sample of the sine distribution. Expressions for the radiated fields are

derived starting from the known fields of a small horizontal loop [4].

While the basic intention of this paper is to present the analytic results, a sampling of results for antennas over a range of shapes is given. A numerical modeling program[1] [5] has been used to find a set of geometries that resonate first at 30 MHz. Free space has been assumed as the antenna environment.

II. EQUATIONS FROM GEOMETRY

A. The Idealized Winding

A mathematically idealized, or simplified, version of the winding is one that has no wire thickness so that the windings lie in the surface of the core. On this basis, Fig. 3 shows the coordinate variables for the core. a is the core major radius and b is the core cross section, or minor, radius. A point on the core surface is defined by cylindrical coordinates ρ, ϕ, z. In order to be able to generate a wire list for NEC [5], to express the winding length, and to reduce the expressions to a function of a single variable, it is convenient to find the coordinates in rectangular form and then express them as functions of one of the angle variables. It is clear from Figs. 1 and 2 that each point in a winding has a unique value of ϕ. If θ is allowed to have values up to $2\pi N$, where N is the number of turns in a winding, then each point in the winding also has a unique value in θ. Indeed

$$\phi = \theta/N. \tag{1}$$

From Fig. 3

$$x = \rho \cos \phi$$
$$y = \rho \sin \phi$$
$$\rho = a + b \cos \theta$$

giving

$$x = (a + b \cos \theta) \cos(\theta/N) \tag{2}$$
$$y = (a + b \cos \theta) \sin(\theta/N) \tag{3}$$
$$z = b \sin \theta. \tag{4}$$

These equations apply to the right winding. The left winding has the same description, except that ϕ goes from 0 to -2π. This means $\phi = -\theta/N$, which changes the sign of y in (3).

It would be extremely useful to have an expression for the total winding length. Let this be L. The incremental length is given by each of the following expressions:

$$(dL)^2 = (dx)^2 + (dy)^2 + (dz)^2$$
$$(dL)^2 = (b\,d\theta)^2 + (\rho\,d\phi)^2.$$

From either expression, the previous equations can be used to reduce dL to a function of θ alone, so that

$$L = \int_0^{2\pi N} \sqrt{b^2 + \frac{1}{N^2}(a + b \cos \theta)^2}\, d\theta. \tag{5}$$

[1]The version used here is version 2 of the source code, compiled for double-precision arithmetic.
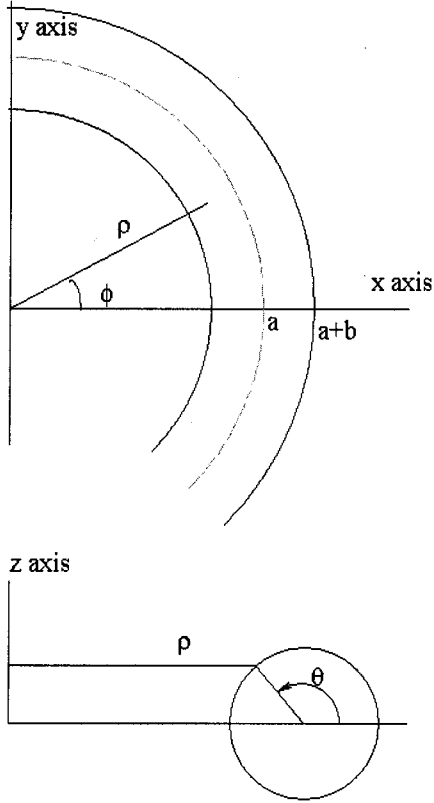
Fig. 3.   Coordinates for the CTHA core.

There is no closed-form solution to this integral. It has to be approximated numerically.

B. Mathematically Approximating a Real Winding

Fig. 4 shows some geometry changes to accommodate real wires. Not only does the wire radius add to b, but the wires overlap on alternating sides along the winding. The overlap is modeled by adding s_1 times a function of θ which is 1 on one side of the core and goes down to zero on the other. The equivalent radius chosen is

$$b_{\text{eq}} = b + r + s_1 \left| \cos\left(\frac{\theta}{2}\right) \right| \qquad (6)$$

for the right winding and

$$b_{\text{eq}} = b + r + s_1 \left| \sin\left(\frac{\theta}{2}\right) \right| \qquad (7)$$

for the left winding.

It is useful for some purposes to have an average value for b_{eq}

$$b_{\text{av}} = \frac{1}{\pi} \int_0^{\pi} b_{\text{eq}} d\theta = b + r + s_1 \frac{2}{\pi}. \qquad (8)$$

The overall diameter is an important issue in antenna design. Counting out from the center and then doubling, one finds

$$D = 2(a + b + 2r + s_1). \qquad (9)$$

The minimum a/b is the condition reached when the turn spacing on the inside of the core s_2 is equal to the minimum
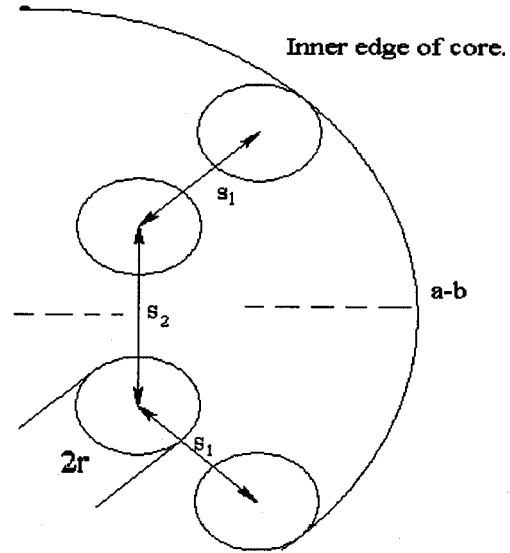
Fig. 4.   Core with wires on it. S_1 is a minimum wire spacing.

allowed wire spacing s_1. For N turns, this gives an inner circumference of Ns_1, so

$$a_{\min} = \frac{Ns_1}{2\pi} + s_1 + r + b_{\text{MAX}}. \qquad (10)$$

Eliminating a between (9) and (10) and solving for b_{MAX} gives the minimum a/b for a specified D and N

$$b_{\text{MAX}} = \frac{D}{4} - \frac{3r}{2} - s_1 \left(\frac{N}{4\pi} + 1 \right). \qquad (11)$$

C. The Elliptical Loop

An ellipse of minor axis $2b$ and major axis $2c$ has, by direct integration of the appropriate formula

$$\text{Area} = \pi bc. \qquad (12)$$

The position and orientation of each loop has to be specified for the field calculations. We also need the loop major axis width. Fig. 5 is a sketch of the top view of two loops (one turn of each winding) with dimensional and angle definitions. Since there are N turns in a winding and one turn from each winding makes two loops, there are N loops in each transmission line. The angle in the x–y plane subtended by each loop, and the center-to-center angle, is $\beta = \pi/N$. The center of the first loop is half this angle off the x axis, so the center for the nth loop is at

$$\phi_n = \frac{\pi}{N}\left(n - \frac{1}{2}\right). \qquad (13)$$

The loop is rotated off the radius line through its center by an angle

$$\phi_p = \frac{\pi}{2N} - \alpha \qquad (14)$$

where α is found from the trigonometry of the figure as follows:

$$h = (a+b)\sin\beta, \ \ d = (a+b)\cos\beta - (a-b)$$

$$\alpha = \tan^{-1}\left(\frac{h}{d}\right), \ \ w = \sqrt{h^2 + d^2}. \qquad (15)$$
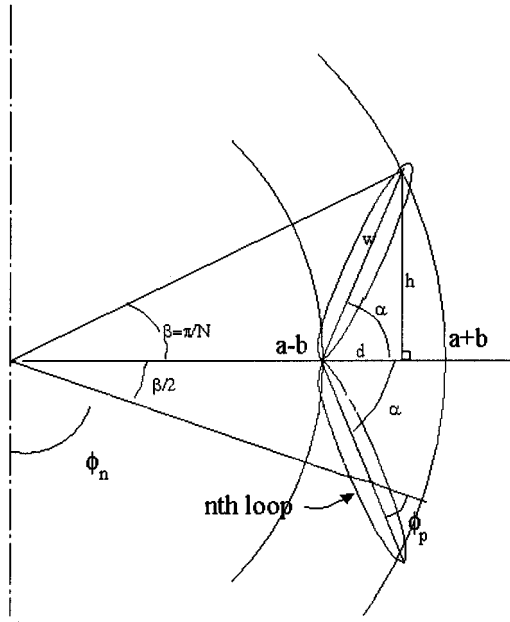
Fig. 5. Geometry of loop orientation and size.

The angle of the loop with respect to a line through its center parallel to the x-axis is

$$\phi_A = \phi_n + (-1)^n \phi_p. \tag{16}$$

III. THE RADIATED FIELD

The fields radiated by a small loop lying in the x–y plane are given in many books on electromagnetics and antennas. In this section, we take this result and transform it to a vertical loop at an angle from the x-axis and then use the parallel-ray approximation to get the far field for the loop displaced from the origin of coordinates. Since the antenna has left–right symmetry about the x-axis, the fields for corresponding loops can be added to reduce the field summing to N terms.

The $\mathbf{E}$ field for a small loop lying in the x–y plane is

$$\mathbf{E} = \frac{MZ_0 k_0^2}{4\pi r} e^{-jk_0 r} \sin(\theta) \mathbf{a}_\phi \tag{17}$$

in which $M = \text{current} \times \text{area}$, k_0 is the wavenumber, $2\pi/\lambda$, r, ϕ and θ are the spherical coordinates for the field point, and $\mathbf{a}_\phi$ is a unit vector.

The key to getting to the final field value for the rotated vertical loop is to get the components in rectangular coordinates. It is useful to use $\rho = \sqrt{x^2 + y^2}$, the cylindrical radius, as well

$$\mathbf{a}_\phi = \mathbf{a}_y \cos\phi - \mathbf{a}_x \sin\phi = \mathbf{a}_y \frac{x}{\rho} - \mathbf{a}_x \frac{y}{\rho}$$

$$\sin\theta = \frac{\rho}{r}.$$

The angle-dependent terms in the field expression are then

$$D = \mathbf{a}_\phi \sin\theta = \mathbf{a}_y \frac{x}{r} - \mathbf{a}_x \frac{y}{r}.$$

This expression only involves the rectangular coordinate values and the radius. Relabeling the axes by a right-handed rotation,

$x \to y, y \to z, z \to x$, converts the loop to vertical position in the z–x plane and gives the angle-dependent terms as

$$D = a_x \frac{z}{r} - a_z \frac{x}{r}.$$

Define

$$E_0 = \frac{MZ_0 k_0^2}{4\pi r} e^{-jk_0 r}. \tag{18}$$

Then, for the loop in the z–x plane

$$E = E_0 \left(a_x \frac{z}{r} - a_z \frac{x}{r} \right).$$

Next we need to shift the loop off the x-axis by an angle ϕ_A. This shifts the horizontal axis of the loop from the x-axis to an x' axis. The field components are then converted to x and y expressions in the new orientation

$$E = E_0 \left(a_{x'} \frac{z}{r} - a_z \frac{x'}{r} \right).$$

The conversions are

$$x' = x\cos\phi_A + y\sin\phi_A, \quad \mathbf{a}_{x'} = \mathbf{a}_x \cos\phi_A + \mathbf{a}_y \sin\phi_A.$$

Putting these into the $\mathbf{E}$ expression gives

$$\mathbf{E} = E_0 \left[\mathbf{a}_x \frac{z}{r} \cos\phi_A + \mathbf{a}_y \frac{z}{r} \sin\phi_A \right.$$
$$\left. - \mathbf{a}_z \left(\frac{x}{r} \cos\phi_A + \frac{y}{r} \sin\phi_A \right) \right].$$

Finally, going back to the observation point angles

$$\frac{x}{r} = \frac{x\rho}{\rho r} = \cos\phi \sin\theta$$

$$\frac{y}{r} = \frac{y\rho}{\rho r} = \sin\phi \sin\theta$$

$$\frac{z}{r} = \cos\theta$$

$$E_x = E_0 \cos\phi_A \cos\theta \tag{19}$$

$$E_y = E_0 \sin\phi_A \cos\theta \tag{20}$$

$$E_z = -E_0 \cos(\phi - \phi_A) \sin\theta. \tag{21}$$

These are the field components for a single vertical loop centered at the origin and turned by an angle ϕ_A from the x axis. The reference current direction was originally $\mathbf{a}_\phi$ and is now $\mathbf{a}_\theta$.

Now we must use the parallel-ray approximation to find the space phase shift due to the fact that each loop is centered at $(r', \phi') = (a, \phi_n)$. The projection of the source point onto the line from the origin to the field point gives

$$r_n = a\cos(\phi - \phi_n)\sin\theta \tag{22}.$$

Since the current in each loop and the loop's orientation and position are functions of its index, it is necessary to subscript those items that depend on n. Taking the nth loop from the right side and the nth loop from the left side, which has $-\phi_{An}$ and $-\phi_n$, and pairing them

$$E_{xn} = E_{0n} \cos\phi_{An} \cos\theta$$
$$\times [e^{jk_0 a \cos(\phi-\phi_n)\sin\theta} + e^{jk_0 a \cos(\phi+\phi_n)\sin\theta}]$$
$$= 2E_{0n} \cos\phi_{An} \cos\theta \cos(k_0 a \sin\phi \sin\phi_n \sin\theta)$$
$$\times e^{jk_0 a \cos\phi \cos\phi_n \sin\theta} \tag{23}$$

$$E_{yn} = 2jE_{0n} \sin\phi_{An} \cos\theta \sin(k_0 a \sin\phi \sin\phi_n \sin\theta)$$
$$\times e^{jk_0 a \cos\phi \cos\phi_n \sin\theta} \tag{24}$$

$$E_{zn} = -2E_{0n} \sin\theta e^{jk_0 a \cos\phi \cos\phi_n \sin\theta}$$
$$\times [\cos\phi_{An} \cos\phi \cos(k_0 a \sin\phi \sin\phi_n \sin\theta)$$
$$+ j\sin\phi_{An} \sin\phi \sin(k_0 a \sin\phi \sin\phi_n \sin\theta)]. \tag{25}$$

Next, we sum the field components from the loop pairs around the antenna. To simplify the notation, define

$$u_n = k_0 a \cos\phi \cos\phi_n \sin\theta \tag{26}$$

$$v_n = k_0 a \sin\phi \sin\phi_n \sin\theta \tag{27}$$

$$P_n = \frac{AI_n Z_0 k_0^2}{2\pi} e^{ju_n}$$
$$= 60 A I_n k_0^2 e^{ju_n} \tag{28}$$

in which $A = $ loop area, I_n is the nth loop current. P_n has the basic amplitude terms, with the propagation factor, $\exp(-jk_0 r)/r$, dropped out. Continuing with definitions

$$U = \sum_{n=1}^{N} P_n \cos\phi_{An} \cos(v_n)$$

$$V = \sum_{n=1}^{N} P_n \sin\phi_{An} \sin(v_n). \tag{29}$$

The total field, in rectangular components, is

$$E_x = U \cos\theta \tag{30}$$

$$E_y = jV \cos\theta \tag{31}$$

$$E_z = -\sin\theta [U \cos\phi + jV \sin\phi]. \tag{32}$$

The final step is to convert to spherical components. By constructing the appropriate triangles, one can find the following conversion formulas:

$$E_\rho = E_x \cos\phi + E_y \sin\phi$$
$$E_\phi = E_y \cos\phi - E_x \sin\phi$$
$$E_r = E_z \cos\theta + E_\rho \sin\theta$$
$$E_\theta = E_\rho \cos\theta - E_z \sin\theta. \tag{33}$$

Applying these results to (30)–(32), we have

$$E_r = 0 \tag{34}$$

$$E_\theta = U \cos\phi + jV \sin\phi \tag{35}$$

$$E_\phi = -\cos\theta [U \sin\phi - jV \cos\phi]. \tag{36}$$

IV. NUMERICAL RESULTS

A. Definitions

Programs have been written which embody all the equations in the previous sections. The results given in the following subsection assume a transmission line current sampled at each loop as

$$I_k = \sin\left(h(k - 0.5)\frac{\pi}{2N}\right) \quad 1 \le k \le N. \tag{37}$$

$h = 1, 2,$ or 3 for first, second, or third resonance. For directivity and gain, the E-field is calculated at the centers of $2°$ steps

over a quarter sphere. Once the E-field is computed, the power density is computed from

$$S = \frac{1}{120\pi}(|E_\theta|^2 + |E_\phi|^2). \tag{38}$$

The total radiated power is

$$P_{\text{rad}} = 4 \sum_{n=1}^{90} \sum_{k=1}^{45} S(k,n) \sin\left(\frac{(k - 0.5)\pi}{90}\right) \left(\frac{\pi}{90}\right)^2. \tag{39}$$

The loss power is calculated from the loop currents and the resistance per turn, R, as

$$P_{\text{loss}} = 2R \sum_{k=1}^{N} \sin^2\left(h(k - 0.5)\frac{\pi}{2N}\right). \tag{40}$$

The directivity is

$$D = \frac{4\pi S_{\text{MAX}}}{P_{\text{rad}}}. \tag{41}$$

The efficiency and gain are

$$\eta = \frac{P_{\text{rad}}}{P_{\text{rad}} + P_{\text{loss}}} \quad \text{and} \quad G = D\eta. \tag{42}$$

B. Shapes and Performance

The antenna patterns have simple shapes up through third resonance. They are determined by the standing-wave current distribution and the space-phase shift across the antenna. At all frequencies, the current distribution has a maximum at the shorted connection of the two transmission lines, opposite the feed point. Below first resonance, the azimuth pattern is the figure-8 of the vertical loop. As first resonance is approached, the notches are filled in and become dips. This is because the space phase shift between waves from the turns with the maximum current, at the rear of the antenna, and the waves from the turns at the sides of the antenna is sufficient to prevent cancellation, and the current at the feed point approaches a minimum. Above first resonance, the current minimum splits into two, one on each side of the feedpoint. As second resonance is approached, these minima go to midway around, to the y axis, and a second maximum is at the feedpoint. This distribution causes cancellation along the y-axis which produces the figure-8 pattern again. As frequency is increased above second resonance the current maximum at the feedpoint splits and three current maxima are formed. At third resonance, there are three maxima and three minima evenly spaced around the antenna. Again, because of current sign changes and space phase differences, the notches become dips. If isotropic patterns are the goal, then operation near first or third resonance is necessary.

The following results are grouped first by the number of turns, 4, 6, 8, or 10, in each winding. Within each group, the ratio of major to minor torus radii, a/b, is held constant at each of several values, and then the radii searched until resonance at 30 MHz is achieved. This search is done using a double-precision version of NEC2 [5]. Two copper conductor sizes are used, 0.5-in and 0.25-in outer diameter. The larger size is used in the 4- and 6-turn groups, and the smaller size is used in another 6-turn and the remaining groups. Efficiency is an important issue for

TABLE I

GEOMETRIES THAT HAVE FIRST RESONANCE AT 30 MHz, FOUND USING NEC2D. η_1 AND η_3 ARE EFFICIENCIES AT FIRST AND THIRD RESONANCES, f_3 IS THIRD RESONANCE FREQUENCY IN MHz. THE ASTERISK, $*$, INDICATES THE ENTRY WITH THE LARGEST MINOR RADIUS IN EACH GROUP

code	a, m	b, m	a/b	η_1, %	$f_{3, \text{MHz}}$	η_3, %
4-turn, ½" copper designs.						
4,2/2	0.1706	0.0853	2	37	98.5	98.4
4,4/2*	0.38	0.095	4	42	90.3	98.6
4,6/2	0.501	0.0835	6	35	89.4	98:3
4,8/2	0.568	0.071	8	30	89	98
6-turn, ½" copper designs.						
6,4/2	0.184	0.046	4	20	96.5	97
6,6/2*	0.318	0.053	6	25	91.3	97
6,8/2	0.4	0.05	8	23	90.3	97
6-turn, ¼" copper designs.						
6,4/4*	0.288	0.072	4	13	92	93
6,6/4	0.414	0.069	6	12	90.5	92
6,8/4	0.496	0.062	8	9.6	90	89
8-turn, ¼" copper designs.						
8,4/4	0.176	0.044	4	6.3	94	87
8,6/4*	0.294	0.049	6	7.6	91	88
8,8/4	0.3816	0.0477	8	7	90.6	87
10-turn, ¼" copper designs.						
10,4/4	0.076	0.019	4	1.9	100	74
10,6/4	0.192	0.032	6	4.4	92.8	82
10,8/4*	0.2792	0.0349	8	5	91.2	83

the CTHA, just as it is for a single small loop, so the conductor is chosen as large as possible for the turn size used.

The performance measures presented are efficiency, dip ratio, directivity, and gain. The dip ratio is $S_{\text{min}}/S_{\text{max}}$. Table I shows the geometries and efficiencies found using NEC2D. Also included in Table I is a labeling code to identify the antennas in the following tables. The code has the form $x, y/z$ in which x is the number of turns per winding, y is a/b, and $/z$ is either $/2$ or $/4$ for 0.5-in– or 0.25-in—diameter copper. Efficiency can be calculated in two ways using NEC2D. The input file was set to give both. The program will calculate the input power from the input current and applied voltage, P_{in}, and the loss power, P_{loss}, by summing I^2R over all the wire segments. The radiated power is found as the difference between these powers and the efficiency reported on this basis. The second method is to have the program calculate the fields over a quarter sphere and report the average gain. If perfect accuracy is present, these two numbers should be the same. For the CTHA this is not the case, especially at and below first resonance. The lower of the two figures is given in Table I.

The following tables give performance results from the analytically derived field formulas for the above shapes. The width and height of each design is also included so that the reader can readily identify the connections between shape and the various performance criteria.

V. DISCUSSION

The first question that needs to be addressed is how good is the model? The general properties of the patterns given by the analytical formulas and by the numerical method are the same. However, the numerical method shows more horizontally polarized radiation at low elevations. This difference is due to the assumption that the loops are completely vertical, which they are not. The efficiencies given by the formulas are in the range of those from NEC2D. At first resonance, the two ways of calculating efficiency in NEC2D have a ratio of about 1.5:1, so that the validity of either is doubtful. At least the formulas do not overestimate efficiency.

There are several things to be said about the effect of shape parameters on performance. The most obvious is that the single most important factor for determining efficiency is the loop radius b. As with ordinary single-turn and cylindrical multi-turn small loops, this radius determines the space-phase difference across the loop and, therefore, the degree to which fields from opposite current-carrying segments do not cancel. The highest efficiency goes with the fewest turns. Increasing the number of turns for a given design frequency means that the phase shift per turn in the current wave must be reduced, which in turn forces a smaller turn.

The effect of a/b is different on different parameters. For a fixed number of turns there is a value either side of which produces less efficiency. This value increases with the number of turns. The dip ratio and directivity also vary with a/b. Dip ratio magnitude appears to decrease with increasing a/b at first resonance. At third resonance, dip ratio magnitude has a minimum at larger values of a/b than the efficiency maximum. One might expect that directivity would decrease with dip magnitude. This is true at first resonance (Table II), but at third resonance (Table III) the opposite seems to happen.

The sizes in this sampling of designs range from about 1×0.3 m for the most efficient 4-turn design down to 0.25×0.1 m for the smallest and least efficient 10-turn design. The wavelengths at first and third resonances are about 10 and 3.3 m.

TABLE II
PERFORMANCE AT FIRST RESONANCE, 30 MHz, $\lambda_1 = 10$ m

Antenna	η, %	dip, dB	D, dB	G, dB	width, m	height, m
4,2/2	53.7	-15.1	1.7	-0.98	0.637	0.295
4,4/2*	59.1	-8.4	1.49	-0.79	1.08	0.315
4,6/2	51.2	-6.1	1.24	-1.68	1.29	0.292
4,8/2	41.5	-4.9	1.01	-2.8	1.4	0.267
6,4/2	36.7	-14.6	1.72	-2.63	0.585	0.217
6,6/2*	42	-10.1	1.64	-2.1	0.867	0.231
6,8/2	38.5	-8.2	1.58	-2.56	1.03	0.225
6,4/4*	27.5	-10.9	1.66	-3.95	0.783	0.207
6,6/4	24.4	-7.9	1.57	-4.57	1.03	0.201
6,8/4	19	-6.5	1.49	-5.72	1.18	0.187
8,4/4	14.7	-15	1.72	-6.6	0.502	0.151
8,6/4*	17.4	-10.7	1.66	-5.93	0.749	0.161
8,8/4	16.1	-8.6	1.6	-6.34	0.921	0.158
10,4/4	4.54	-22	1.75	-11.7	0.253	0.101
10,6/4	10.3	-14.3	1.72	-8.18	0.51	0.127
10,8/4*	11.7	-11.2	1.67	-7.66	0.691	0.132

TABLE III
PERFORMANCE AT THIRD RESONANCE, λ_3 IS BETWEEN 3 AND 3.37 m

Antenna	η, %	Dip, dB	D, dB	G, dB	width, m	height, m
4,2/2	99.5	-10.5	1.83	1.81	0.637	0.295
4,4/2*	99.3	-3.65	1.54	1.52	1.08	0.315
4,6/2	99.1	-6.8	2.3	2.25	1.29	0.292
4,8/2	98.7	-10.2	3.3	3.2	1.4	0.267
6,4/2	99.1	-12.4	1.9	1.86	0.585	0.217
6,6/2*	99	-8.12	2.12	2.08	0.867	0.231
6,8/2	98.6	-6.28	2.3	2.24	1.03	0.225
6,4/4*	98.2	-8.9	2.1	2	0.783	0.207
6,6/4	97.3	-6.12	2.33	2.22	1.03	0.201
6,8/4	96	-6.22	2.5	2.33	1.18	0.187
8,4/4	96.7	-13.2	1.89	1.74	0.502	0.151
8,6/4*	96.7	-9.21	2.09	1.94	0.749	0.161
8,8/4	95.9	-7.18	2.3	2.11	0.921	0.158
10,4/4	91.3	-19.7	1.79	1.39	0.253	0.101
10,6/4	94.8	-12.6	1.91	1.68	0.51	0.127
10,8/4*	94.7	-9.8	2.05	1.81	0.691	0.132

Many different applications are possible depending on which characteristics are most important. For example, if it is important to have a low-profile low-directivity surface-mounted antenna, the 10-turn third-resonance design has a reasonable efficiency at a height of less than a 30th of a wavelength. Furthermore, it could be operated at the inductive side of resonance, so that it could be tuned with a high-efficiency capacitor, unlike the short whip which requires an inherently inefficient coil for tuning.

An application requiring minimum dip ratio would need more study. The sampling of a/b values used here is too coarse. It may very well be that a dip magnitude minimum exists in the third resonance designs, and it may be that zero dip is possible at either resonance. Software to address these matters in a timely manner hasn't been written yet.

VI. OTHER ISSUES AND POSSIBILITIES

The fact that a standard numerical method and the analytical formulas given in this paper agree qualitatively makes them mu-

tually validating to that extent. Carefully controlled experiments based on these designs needs to be performed to provide the third leg of validation.

NEC, in its various versions, is a general-purpose antenna code designed for moderate-sized antennas and large structures. A code with limited objectives can be written in a more specialized way to give greater accuracy. For example, a code, still in development, which uses the Fourier Series for both basis and weighting functions has been written which produces better than 90% agreement between input power calculated from input voltage and current, and input power as the sum of loss and radiated powers.

An important practical problem with the CTHA is its high and very reactive impedance near the odd-numbered resonances. Advantage can be taken of its transmission-line aspect by treating the connections opposite the feed port as a second port. Open-circuiting the cross-tie forces the current maximum at first and third resonance to be at the input terminals, without changing the patterns. This change makes

these resonances low-impedance which may make them easier to match. Lumped-element loading at the second port, and at the wire crossings, may also provide some useful effects on both impedance and pattern bandwidth. A casual numerical experiment in which a smaller CTHA was connected to port 2 of a 200-MHz first-resonance design showed improved pattern uniformity over an octave.

All the work reported here is for a CTHA with an air core. Most of the experimental work has been done on designs with dielectric cores and has been fraught with problems. Analytical treatment of the dielectric core case is currently beyond this author's capability. The preliminary code mentioned above is aimed at this case. The code is currently much slower than it needs to be and strains the memory capacities of computers available to this investigator. However, some interesting correlations have been found between its numerical results and physical experiments. With a dielectric core present, the resonant frequencies decrease, as expected, the efficiency increases, the horizontally polarized field increases, and the azimuth pattern skews. The latter effects can be understood by realizing that the dielectric is driven by the near field of the wires, so that it is also radiating. The atomic dipoles near a wire will have their axes perpendicular to the wire and radiate fields perpendicular to those of the wire. The actual geometric situation is very complex, but this notion may explain the large amount of horizontally polarized radiation at low elevation when a dielectric core is present.

In conclusion, the analytical approach has led to some useful formulas and a perspective that points the way to further development of this very interesting antenna type.

REFERENCES

[1] K. L. Van Voorhies and J. E. Smith, "Toroidal Antenna," U.S. Patent 5 442 369, Aug. 15, 1995.
[2] K. L. Van Voorhies, "Contrawound Toroidal Helical Antenna," U.S. Patent 5 734 353, Mar. 31, 1998.
[3] D. B. Miron, "A study of the CTHA based on analytical models," Rep. Emergent Technologies Corp., Mt. Clare, WV, Aug. 1996.
[4] J. D. Kraus, *Antennas*. New York: McGraw-Hill, 1988.
[5] G. Burke and A. Poggio, Numerical Electromagnetics Code (NEC)-Method of Moments, NOSC TD 116, Jan. 1981.

Douglas B. Miron (S'58–M'66–SM'94) received the B.E. and M.E. degrees in electrical engineering from Yale University, New Haven, CT, in 1962 and 1963, respectively, and the Ph.D. degree in electrical engineering/control and communications from the University of Connecticut, Westport, in 1977.

He worked in industry from 1963 to 1967; from 1970 to 1979, and 1997. He taught at South Dakota State University from 1979 through 1996 and has been consulting since 1998. He has worked, taught, and published in nearly every major area of electrical engineering. His current interests are in small antennas and RF circuits.